

AD-A181 546

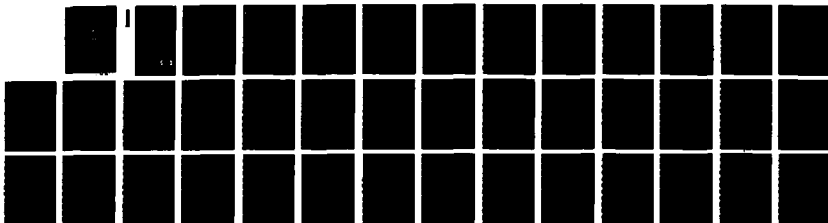
ANALYTICAL MODELS OF CONDUCTIVITY-CHANNEL TRACKING(U)  
SCIENCE APPLICATIONS INTERNATIONAL CORP SAN DIEGO CA  
B B GODFREY ET AL 04 APR 87 N68921-85-C-0044

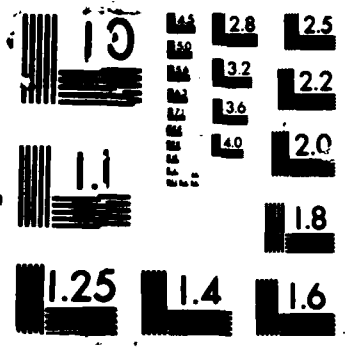
1/1

UNCLASSIFIED

F/G 20/7

NL





DTIC FILE COPY

12

AMRC-R-899  
Copy 117

ANALYTICAL MODELS OF CONDUCTIVITY-CHANNEL TRACKING

Brendan B. Godfrey  
Dale R. Welch

April 1987

Sponsored by: DEFENSE ADVANCED RESEARCH PROJECTS AGENCY  
Monitored by Naval Surface Weapons Center under  
Contract N60921-85-C-0044 to SAIC

and

Science Applications International Corporation  
Subcontract 15-860022-79

Prepared by: MISSION RESEARCH CORPORATION  
1720 Randolph Road, S.E.  
Albuquerque, New Mexico 87106

APPROVED FOR PUBLIC RELEASE

DTIC  
ELECTE  
S JUN 24 1987 D  
E

87 6 23 003

UNCLASSIFIED

AD A 181 546

SECURITY CLASSIFICATION OF THIS PAGE

REPORT DOCUMENTATION PAGE

1a. REPORT SECURITY CLASSIFICATION Unclassified		1b. RESTRICTIVE MARKINGS		
2a. SECURITY CLASSIFICATION AUTHORITY		3. DISTRIBUTION/AVAILABILITY OF REPORT		
2b. DECLASSIFICATION/DOWNGRADING SCHEDULE				
4. PERFORMING ORGANIZATION REPORT NUMBER(S) AMRC-R-899		5. MONITORING ORGANIZATION REPORT NUMBER(S)		
6a. NAME OF PERFORMING ORGANIZATION Mission Research Corporation	6b. OFFICE SYMBOL (if applicable) AMRC	7a. NAME OF MONITORING ORGANIZATION		
6c. ADDRESS (City, State, and ZIP Code) 1720 Randolph Road, S.E. Albuquerque, New Mexico 87106-4245		7b. ADDRESS (City, State, and ZIP Code)		
8a. NAME OF FUNDING/SPONSORING ORGANIZATION Naval Surface Weapons Center	8b. OFFICE SYMBOL (if applicable)	9. PROCUREMENT INSTRUMENT IDENTIFICATION NUMBER		
8c. ADDRESS (City, State, and ZIP Code) 10901 New Hampshire Avenue White Oak Silver Spring, Maryland 20903-5000		10. SOURCE OF FUNDING NUMBERS		
		PROGRAM ELEMENT NO	PROJECT NO	TASK NO
11. TITLE (Include Security Classification) ANALYTICAL MODELS OF CONDUCTIVITY-CHANNEL TRACKING				
12. PERSONAL AUTHOR(S) Brendan B. Godfrey and Dale R. Welch				
13a. TYPE OF REPORT	13b. TIME COVERED FROM TO	14. DATE OF REPORT (Year, Month, Day) 1987 April 04	15. PAGE COUNT 34	
16. SUPPLEMENTARY NOTATION				
17. COSATI CODES		18. SUBJECT TERMS (Continue on reverse if necessary and identify by block number)		
FIELD	GROUP			SUB-GROUP
19. ABSTRACT (Continue on reverse if necessary and identify by block number) A new analytical model for the tracking force on an ultrarelativistic electron beam in a conductivity channel is derived from the complete Frozen Field Equations. The model assumes the beam to be entirely within a sharp-edged constant conductivity channel. Axial return currents are ignored except at the channel boundary, and the drift tube wall is assumed to be at large radius. It is shown, however, that these latter restrictions are not serious, although a small drift tube radius may complicate measurement of the tracking force. This Frozen Field Tracking Model reduces to the Electrostatic Tracking Model in the appropriate limit, but in other cases predicts slightly larger, sometimes oscillatory forces. The analysis also indicates that magnetic fields can play a positive role in tracking. For completeness, channel tracking forces for the New Field Equations with and without an axial displacement current are derived. With the displacement current the New				
20. DISTRIBUTION/AVAILABILITY OF ABSTRACT <input type="checkbox"/> UNCLASSIFIED/UNLIMITED <input type="checkbox"/> SAME AS RPT <input type="checkbox"/> DTIC USERS		21. ABSTRACT SECURITY CLASSIFICATION Unclassified		
22a. NAME OF RESPONSIBLE INDIVIDUAL		22b. TELEPHONE (include Area Code)	22c. OFFICE SYMBOL	

19. Concluded

Field Equations exhibit tracking qualitatively similar to that of the full Frozen Field Equations, while without it they exhibit tracking as described by the Electrostatic Tracking Model.



## ACKNOWLEDGMENTS

We are grateful to W. Fawley, R. Fernsler, J. Freeman, B. Hui, K. O'Brien, D. Mitrovich, and S. Yu for advice and friendly criticism. This research is supported by the Defense Advanced Research Projects Agency and monitored by the Naval Surface Weapons Center.

<b>Accession For</b>	
NTIS GRA&I	<input checked="" type="checkbox"/>
DTIC TAB	<input type="checkbox"/>
Unannounced	<input type="checkbox"/>
Justification	
<b>By</b>	
<b>Distribution/</b>	
<b>Availability Codes</b>	
<b>Dist</b>	<b>Avail and/or Special</b>
A-1	



## CONTENTS

<u>Chapter</u>		<u>Page</u>
1	INTRODUCTION . . . . .	1
2	ELECTROSTATIC TRACKING MODEL . . . . .	5
3	FROZEN FIELD TRACKING MODEL . . . . .	9
4	CHANNEL TRACKING WITH THE NEW FIELD EQUATIONS . . . . .	20
5	DIFFUSION CORRECTIONS . . . . .	24
6	CONDUCTING-WALL CORRECTIONS . . . . .	29
7	CONCLUSIONS . . . . .	32
	REFERENCES . . . . .	34

## ILLUSTRATIONS

<u>Figure</u>		<u>Page</u>
1	ELECTRON BEAM IN SHARP EDGED CONDUCTIVITY CHANNEL OF RADIUS $a$ AND DRIFT TUBE OF RADIUS $b$ . THE BEAM CENTROID IS DISPLACED FROM THE CHANNEL AND DRIFT TUBE AXIS BY A SMALL DISTANCE $\epsilon$ . . . . .	6
2	THE FROZEN FIELD TRACKING MODEL NORMALIZED FORCE ( $-\alpha$ FROM EQ. 47) ON A 10 kA, 15 cm RISE LENGTH, 0.5 cm RADIUS BEAM OFFSET $\epsilon = 0.25$ cm IN AN $a = 1$ cm, $\sigma = 1$ cm <sup>-1</sup> CONSTANT CONDUCTIVITY CHANNEL FOR $x = 0, 1, 2,$ and 5. THE $x = 0$ LIMIT CORRESPONDS TO THE ELECTROSTATIC TRACKING MODEL RESULT . . . . .	17
3	THE ELECTRIC AND MAGNETIC COMPONENTS OF THE NORMALIZED TRACKING FORCE ON A 10 kA, 15 cm RISE LENGTH, 0.5 cm RADIUS BEAM OFFSET $\epsilon = 0.25$ cm IN AN $a = 1$ cm, $\sigma = 0.5$ cm <sup>-1</sup> CONSTANT CONDUCTIVITY CHANNEL FOR $x = 1$ . THE FORCES ARE OBTAINED BOTH FROM EQUATIONS 51 AND 52 AND FROM A COMPARABLE IPROP SIMULATION . . . . .	18

## CHAPTER 1 INTRODUCTION

IPROP channel tracking simulations<sup>1</sup> of fast rise time beams in conductivity channels typically predict much stronger tracking forces than those of previously published computational studies.<sup>2,3</sup> Moreover, the forces are predominantly magnetic, whereas the pivotal analytical model in use had assumed,<sup>4</sup> and the earlier computational studies found, only electrostatic tracking forces.

Recent investigations<sup>5,6</sup> suggest that the larger tracking forces in IPROP are in part due to differences in the chemistry model used and the beam profiles assumed. For instance, IPROP employs a temperature dependent momentum transfer cross section which increases by as much as a factor of three as the channel temperature rises due to the presence of the beam head.<sup>7</sup> However, significant qualitative and quantitative discrepancies between the tracking results of IPROP and the other three-dimensional propagation codes persist even after chemistry and beam profiles differences are taken into account.

These remaining discrepancies seem to be caused by the different electromagnetic field models used in the codes. IPROP<sup>8</sup> solves the complete set of Maxwell's equations in a Galilean-transformed frame moving with the beam. Alternatively, IPROP can solve the Frozen Field Equations, which are obtained from Maxwell's equations by assuming the fields in a Galilean-transformed frame moving with the beam at the speed of light are independent of time. For relativistic beams the tracking forces are essentially the same in both cases. RINGBEARER II<sup>9</sup> and DYNASTY II,<sup>10</sup> on the other hand, utilize the New Field Equations,<sup>11</sup> an approximation to the Frozen Field Equations which includes only the scalar potential and axial component of the vector potential with no displacement current. A recent modification to DYNASTY II reintroduces the axial displacement current, which often increases the tracking forces seen in that code.<sup>5</sup>

To clarify the impact of various electromagnetic field approximations on conductivity-channel tracking, we have developed analytical tracking models for the Frozen Field Equations, for the New Field Equations, and for the New Field Equations plus the axial displacement current. As in the original Electrostatic Tracking Model,<sup>4</sup> the channel conductivity is assumed constant in space and time within the channel, which has a sharp edge, and the beam is contained entirely within the channel. Although somewhat artificial, these assumptions seem to capture much of the essential tracking phenomena while making the calculations analytically tractable. Extending the models to accommodate smoothly varying radial conductivity profiles is desirable.

The Frozen Field Tracking Model reproduces well the results of IPROP when the code is run under the same conditions.<sup>1</sup> In particular, the model correctly predicts strong magnetic tracking and electric detracking, with the former dominant, very early in the beam pulse. As a certain quantity  $\underline{X}$ , to be defined later, goes to zero, the model equations reduce to those of the Electrostatic Tracking Model. Even for moderate  $\underline{X}$  the total tracking force from the Frozen Field Tracking Model typically agrees with the force from the Electrostatic Tracking Model to within a factor of two, although, of course, there is no agreement at all between the electric and magnetic components of the forces in the two models. Approximate agreement between the total forces arises from the near cancellation of the electric and magnetic forces in Frozen Field Tracking Model. Whether the agreement persists for more realistic channel conditions is uncertain.

Quite surprisingly, the tracking model based on the New Field Equations with an axial displacement current gives electric and magnetic tracking force equations formally identical to those of the Frozen Field Tracking Model but with  $\underline{X}$  different by about a factor of two. The tracking model for the New Field Equations without an axial displacement current, on the other hand, turns out to be the same as the Electrostatic Tracking Model.

This report describes in detail the derivation of the Frozen Field Tracking Model and presents sample predictions. In addition, it outlines corresponding derivations for the New Field Equations with and without an axial displacement current. The derivations are straightforward but lengthy. Source-free dipole fields are determined in the regions inside and outside the channel. The beam fields then are derived without consideration of the channel boundary. Matching the three fields at the channel boundary determines coefficients appearing in the source-free solutions, and the interior source-free solution integrated over the beam cross section gives the dipole tracking force. Because the derivation involves only a two-term expansion in azimuthal angle, it is strictly valid only for small displacements of the beam from the channel axis. However, IPROP simulations suggest that the models are accurate for larger displacements, provided, of course, that the beam remains in the channel.

The material is organized as follows. In Chapter 2 the Electrostatic Tracking Model is rederived using the procedure just outlined in order to illustrate this procedure in a simple case and to provide a basis for subsequent comparisons with the other models. Chapter 3 contains the main results of the report. The Frozen Field Equations are collected and cast as a coupled pair of two-dimensional diffusion equations. For analytical tractability, the diffusion terms then are dropped, and the equations solved to obtain the electric, magnetic, and total tracking forces. Various limits are considered, including the Electrostatic Tracking Model. This same approach is applied to the New Field Equations in Chapter 4. As already noted, it leads to the Frozen Field Tracking Model with  $\chi$  redefined when the axial displacement current is retained and to the Electrostatic Tracking Model when it is not. Neglecting the diffusion terms is justified in Chapter 5. The diffusion equations are Laplace-transformed in the axial direction and solved by a procedure similar, but not identical, to that used in earlier sections. A low frequency expansion then recovers the transforms of the earlier results and provides an estimate of their range of validity. The derivations in Chapters 2 and 3 also assume that the radius of the experimental chamber is large compared to the radius of

the channel. The effects of a smaller chamber are estimated in Chapter 6. Conclusions, including a partial physical explanation of the predicted tracking behavior, are provided in Chapter 7.

The electron charge and mass, and the speed of light are set equal to unity throughout the report. A factor of  $4\pi$  is absorbed into the conductivity  $\sigma$  and the beam density.

CHAPTER 2  
ELECTROSTATIC TRACKING MODEL

Lee's Electrostatic Tracking Model<sup>4</sup> considers a rigid, axisymmetric electron beam propagating in a sharp edged, axisymmetric, constant conductivity channel of radius  $\underline{a}$ . The beam is entirely within the channel and offset slightly from its axis by a distance  $\epsilon$ , as depicted in Figure 1. (The drift tube, of radius  $\underline{b}$ , plays no explicit role in this chapter.)

Computations are performed in the beam frame, assumed to move at the speed of light. The electrostatic potential  $\phi$  is determined from

$$\nabla_{\perp}^2 \phi = -\rho + \rho_c \quad (1)$$

$\rho$  and  $\rho_c$  are the beam and channel plasma charge densities, the latter given by<sup>4</sup>

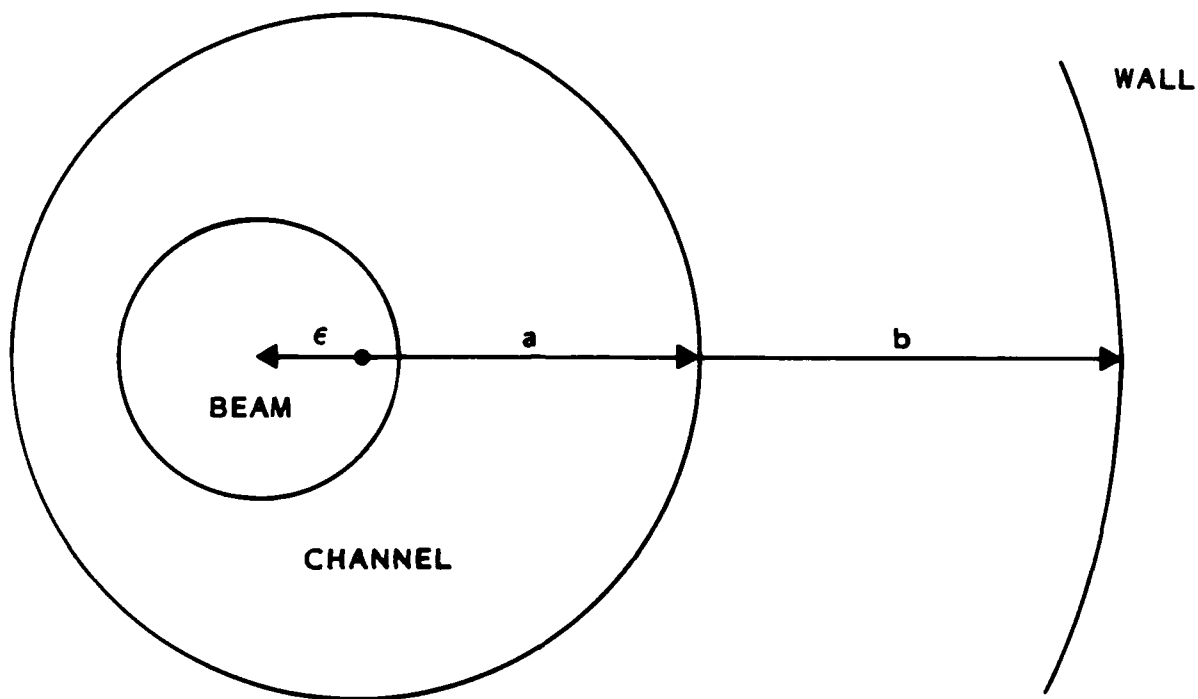
$$\frac{\partial}{\partial \tau} \rho_c + \nabla_{\perp} \cdot \sigma \nabla_{\perp} \phi = 0 \quad (2)$$

$\sigma$  is the channel conductivity.  $\tau$  represents axial distance measured back from the head of the beam (i.e.,  $\tau = t - z$ ), and  $\underline{r}$  and  $\theta$  have their usual meanings in cylindrical coordinates.  $\nabla_{\perp}$  is the transverse (i.e.,  $\underline{r}$  and  $\theta$ ) gradient operator.

Combining Equations 1 and 2 yields

$$\frac{\partial}{\partial \tau} \nabla_{\perp}^2 \phi + \nabla_{\perp} \cdot \sigma \nabla_{\perp} \phi = -\frac{\partial}{\partial \tau} J \quad (3)$$

where  $\rho$  has been replaced by  $J$ , the beam axial current density, for notational consistency with subsequent chapters. (The two quantities are equal for the rigid, ultrarelativistic beam.) Both inside and outside the channel, where  $\sigma$  is constant, Equation 3 can be integrated once in  $\tau$ .



R-899

FIGURE 1. ELECTRON BEAM IN SHARP EDGED CONDUCTIVITY CHANNEL OF RADIUS  $a$  AND DRIFT TUBE RADIUS OF  $b$ . THE BEAM CENTROID IS DISPLACED FROM THE CHANNEL AND DRIFT TUBE AXIS BY A SMALL DISTANCE  $\epsilon$ .

$$\nabla_{\perp}^2 \phi = - \int_0^{\tau} e^{-\sigma(\tau-\tau')} \frac{\partial}{\partial \tau'} J \, d\tau' \quad (4)$$

The radial derivative of  $\phi$  may be discontinuous at the channel boundary due to surface charges. From Equation 3,

$$\frac{\partial}{\partial \tau} \frac{\partial}{\partial r} \phi^{(e)} = \left( \frac{\partial}{\partial \tau} + \sigma \right) \frac{\partial}{\partial r} \phi^{(i)} \quad (5)$$

The potential itself is continuous.

$$\phi^{(e)} = \phi^{(i)} \quad (6)$$

Equations 4-6 are now solved for the force acting on the beam. The dipole (e.g., varying as  $\cos\theta$ ) component of  $\phi$  inside the channel,

$$\phi^{(i)} = \alpha r + S \quad (7)$$

consists of two terms.  $S$  is the dipole potential of the beam in a uniform conductivity background without a boundary. Thus, it contributes nothing to the tracking force. Outside the beam,

$$S = 2 \frac{\epsilon}{r} \int_0^{\tau} e^{-\sigma(\tau-\tau')} \frac{\partial}{\partial \tau'} I \, d\tau' \quad (8)$$

$I(\tau)$  is the beam current, the integral of  $J$  over the beam cross section. The second term,  $\alpha r/a$ , is generated by surface charges at the channel boundary. Outside the channel the dipole potential is simply,

$$\phi^{(e)} = \gamma \frac{a^2}{r} \quad (9)$$

Like  $\alpha$ ,  $\gamma$  is an unknown function of  $\tau$  to be determined.

Inserting Equations 7 and 9 into the boundary conditions, Equations 5 and 6, provides a differential equation for  $\alpha$ .

$$\left(2 \frac{\partial}{\partial \tau} + \sigma\right) \alpha = \frac{\sigma}{a} S \quad (10)$$

Its solution is

$$\alpha = \frac{2\epsilon}{a^2} \int_0^{\tau} \left( e^{-\sigma(\tau-\tau')/2} - e^{-\sigma(\tau-\tau')} \right) \frac{\partial}{\partial \tau'} I \, d\tau' \quad (11)$$

The corresponding dipole electric fields  $E_r$  and  $E_\theta$  are given by  $-\alpha \cos\theta$  and  $-\alpha \sin\theta$ , respectively. Averaged over the beam cross section and added, they give the tracking force,  $-\alpha I$ . This is indeed the result derived by a different route in Reference 4. (Actually, Lee's expression is slightly more general in that it allows  $\sigma$  to vary with  $\tau$ .) The negative sign indicates that the force is inward. Physically, plasma electrons repelled by the beam first accumulate preferentially at the channel edge closest to the beam at the rate  $\sigma$  and then redistribute themselves uniformly around the channel edge at the rate  $\sigma/2$ . Tracking persists in this model as long as  $\partial I / \partial \tau > 0$ .

CHAPTER 3  
FROZEN FIELD TRACKING MODEL

The Frozen Field Equations are a simplified form of Maxwell's equations obtained by performing a Galilean transformation to a frame moving at the speed of light and then dropping time derivatives.

$$\frac{\partial}{\partial \tau} E_z = \frac{1}{r} \frac{\partial}{\partial r} r B_\theta - \frac{1}{r} \frac{\partial}{\partial \theta} B_r - \sigma E_z - J_z \quad (12)$$

$$\frac{\partial}{\partial \tau} B_z = -\frac{1}{r} \frac{\partial}{\partial r} r E_\theta + \frac{1}{r} \frac{\partial}{\partial \theta} E_r \quad (13)$$

$$\frac{\partial}{\partial \tau} (E_r - B_\theta) = -\frac{\partial}{\partial r} E_z \quad (14)$$

$$\frac{\partial}{\partial \tau} (E_r - B_\theta) = \frac{1}{r} \frac{\partial}{\partial \theta} B_z - \sigma E_r - J_r \quad (15)$$

$$\frac{\partial}{\partial \tau} (E_\theta + B_r) = -\frac{1}{r} \frac{\partial}{\partial \theta} E_z \quad (16)$$

$$\frac{\partial}{\partial \tau} (E_\theta + B_r) = -\frac{\partial}{\partial r} B_z - \sigma E_\theta - J_\theta \quad (17)$$

These equations must be used with care, since their derivation involves the implicit assumption that sources move at the speed of light. Nonphysical behavior sometimes arises near infinite conductivity surfaces, and electromagnetic shock waves are possible. Nonetheless, the Frozen Field Equations have been used successfully in many particle beam propagation calculations. As noted in the Introduction, IPROP channel tracking simulations show negligible change (except for beams passing through metal foils) when Maxwell's equations are replaced by the Frozen Field Equations.

For  $\sigma \neq 0$ , it is convenient to combine Equations 12-17 into a pair of second order equations for  $E_z$  and  $B_z$ , analogous to the usual equations describing electromagnetic fields in waveguides.

$$\begin{aligned} \frac{\partial}{\partial \tau} \left( \frac{\partial}{\partial \tau} + \sigma \right) E_z = & \left[ \frac{1}{r} \frac{\partial}{\partial r} r \left( 1 + \frac{\partial}{\partial \tau} \frac{1}{\sigma} \right) \frac{\partial}{\partial r} + \frac{1}{r} \frac{\partial}{\partial \theta} \left( 1 + \frac{\partial}{\partial \tau} \frac{1}{\sigma} \right) \frac{1}{r} \frac{\partial}{\partial \theta} \right] E_z \\ & + \frac{\partial}{\partial \tau} \left[ \frac{1}{r} \frac{\partial}{\partial r} r \frac{1}{\sigma} \frac{1}{r} \frac{\partial}{\partial \theta} - \frac{1}{r} \frac{\partial}{\partial \theta} \frac{1}{\sigma} \frac{\partial}{\partial r} \right] B_z - \frac{\partial}{\partial \tau} J_z \end{aligned} \quad (18)$$

$$\begin{aligned} \frac{\partial}{\partial \tau} B_z = & \left[ \frac{1}{r} \frac{\partial}{\partial r} r \frac{1}{\sigma} \frac{\partial}{\partial r} + \frac{1}{r} \frac{\partial}{\partial \theta} \frac{1}{\sigma} \frac{1}{r} \frac{\partial}{\partial \theta} \right] B_z \\ & - \left[ \frac{1}{r} \frac{\partial}{\partial r} r \frac{1}{\sigma} \frac{1}{r} \frac{\partial}{\partial \theta} - \frac{1}{r} \frac{\partial}{\partial \theta} \frac{1}{\sigma} \frac{\partial}{\partial r} \right] E_z \end{aligned} \quad (19)$$

Transverse beam currents,  $J_r$  and  $J_\theta$ , have been dropped, consistent with the assumptions presented in Chapters 1 and 2. Once the longitudinal fields are determined, the transverse field are obtained from

$$E_r = \frac{1}{\sigma} \left( \frac{\partial}{\partial r} E_z + \frac{1}{r} \frac{\partial}{\partial \theta} B_z \right) \quad (20)$$

$$E_\theta = -\frac{1}{\sigma} \left( \frac{\partial}{\partial r} B_z - \frac{1}{r} \frac{\partial}{\partial \theta} E_z \right) \quad (21)$$

$$\frac{\partial}{\partial \tau} B_r = \frac{\partial}{\partial \tau} \frac{1}{\sigma} \frac{\partial}{\partial r} B_z - \left( 1 + \frac{\partial}{\partial \tau} \frac{1}{\sigma} \right) \frac{1}{r} \frac{\partial}{\partial \theta} E_z \quad (22)$$

$$\frac{\partial}{\partial \tau} B_\theta = \left( 1 + \frac{\partial}{\partial \tau} \frac{1}{\sigma} \right) \frac{\partial}{\partial r} E_z + \frac{\partial}{\partial \tau} \frac{1}{\sigma} \frac{1}{r} \frac{\partial}{\partial \theta} B_z \quad (23)$$

Equations 18 and 19 simplify greatly for constant conductivity. If  $\sigma$  is independent of  $r$  and  $\theta$ , the equations decouple. If, in addition,  $\sigma$  is independent of  $\tau$ , Equation 18 can be integrated once.

$$\left[ \sigma \frac{\partial}{\partial \tau} - \frac{1}{r} \frac{\partial}{\partial r} r \frac{\partial}{\partial r} - \frac{1}{r^2} \frac{\partial^2}{\partial \theta^2} \right] E_z = -\sigma \int_0^\tau e^{-\sigma(\tau-\tau')} \frac{\partial}{\partial \tau'} J \, d\tau' \quad (24)$$

$$\left[ \sigma \frac{\partial}{\partial \tau} - \frac{1}{r} \frac{\partial}{\partial r} r \frac{\partial}{\partial r} - \frac{1}{r^2} \frac{\partial^2}{\partial \theta^2} \right] B_z = 0 \quad (25)$$

Both are two-dimensional diffusion equations. Note the similarity between Equation 24 and Equation 4.

Equations 24 and 25 can be solved exactly inside the channel using Green's functions or Laplace transforms. However, the formal solution which results involves integrals with complicated kernels and is not particularly enlightening. Instead, we obtain an approximate solution by dropping the diffusion terms  $\sigma \partial/\partial \tau$  and treating the simplified equations by the method used in the preceding Chapter. Omitting the diffusion terms in Equations 24 and 25 is reasonable, if fields change in  $\tau$  on a scale slow compared to  $\sigma a^2$ . The range of validity of this approximation is estimated in Chapter 5, where the Laplace transformation solution is obtained and then expanded in powers of the transform variable. Comparing the approximate analytical solution with IPROP computations presented later also supports dropping the diffusion terms.

With the  $\sigma \partial/\partial \tau$  omitted, Equations 24 and 25 become

$$\nabla_{\perp}^2 E_z = \sigma \int_0^{\tau} e^{-\sigma(\tau-\tau')} \frac{\partial}{\partial \tau'} J \, d\tau' \quad (26)$$

$$\nabla_{\perp}^2 B_z = 0 \quad (27)$$

Their dipole solutions are

$$E_z^{(i)} = \frac{\partial}{\partial \tau} \alpha r - \sigma S \quad (28)$$

$$B_z^{(i)} = \frac{\partial}{\partial \tau} \beta r \quad (29)$$

$E_z$  is taken to vary as  $\cos\theta$ , in which case  $E_r$  and  $B_{\theta}$  also vary as  $\cos\theta$ , and  $B_z$ ,  $E_{\theta}$  and  $B_r$  vary as  $\sin\theta$ . Derivatives of the  $\tau$ -dependent unknown functions  $\alpha$  and  $\beta$ , rather than the functions themselves, are introduced to simplify notation later in the calculation.  $\underline{S}$  was introduced in Chapter 2

and is expressed by Equation 8 for that portion of the channel outside the beam.

Equations 18-23 cannot be used outside the channel, because their derivation involves division by  $\sigma$ . Simply multiplying those equations by  $\sigma$  before setting it to zero leaves an incomplete system of equations. In essence, the Frozen Field Equations are qualitatively different in vacuum and in resistive plasma.

Rearranging Equations 12-17 to evaluate the fields outside the channel proceeds as follows. As before, the longitudinal field components are easily isolated.

$$\nabla_{\perp}^2 E_z = \nabla_{\perp}^2 B_z = 0 \quad (30)$$

However,  $E_z$  and  $B_z$  no longer are independent. From Equations 14 and 15,

$$\frac{\partial}{\partial r} E_z + \frac{1}{r} \frac{\partial}{\partial \theta} B_z = 0 \quad (31)$$

In consequence, the transverse field components are only partly determined by  $E_z$  and  $B_z$ .

$$\frac{\partial}{\partial \tau} \left( \frac{1}{r} \frac{\partial}{\partial r} r B_{\theta} + \frac{1}{r} \frac{\partial}{\partial \theta} E_{\theta} \right) = \left( \frac{\partial^2}{\partial \tau^2} - \frac{1}{r^2} \frac{\partial^2}{\partial \theta^2} \right) E_z \quad (32)$$

$$\frac{\partial}{\partial \tau} \left( -\frac{1}{r} \frac{\partial}{\partial r} r E_{\theta} + \frac{1}{r} \frac{\partial}{\partial \theta} B_{\theta} \right) = \left( \frac{\partial^2}{\partial \tau^2} - \frac{1}{r^2} \frac{\partial^2}{\partial \theta^2} \right) B_z \quad (33)$$

$$\frac{\partial}{\partial \tau} \left( \frac{1}{r} \frac{\partial}{\partial r} r E_r - \frac{1}{r} \frac{\partial}{\partial \theta} B_r \right) = \left( \frac{\partial^2}{\partial \tau^2} - \frac{1}{r} \frac{\partial}{\partial r} r \frac{\partial}{\partial r} \right) E_z \quad (34)$$

$$\frac{\partial}{\partial \tau} \left( \frac{1}{r} \frac{\partial}{\partial r} r B_r + \frac{1}{r} \frac{\partial}{\partial \theta} E_r \right) = \left( \frac{\partial^2}{\partial \tau^2} - \frac{1}{r} \frac{\partial}{\partial r} r \frac{\partial}{\partial r} \right) B_z \quad (35)$$

From Equations 30 and 31, the dipole longitudinal fields are

$$E_z^{(e)} = B_z^{(e)} = \frac{\partial}{\partial \tau} \gamma \frac{a^2}{r} \quad (36)$$

if  $a^2/b^2 \ll 1$ . Of the dipole transverse fields, only the combination  $E_\theta - B_\theta$  is needed to derive the tracking force in the large radius drift tube limit. It is described by

$$\frac{\partial}{\partial \tau} \frac{\partial}{\partial r} (E_\theta - B_\theta) = - \left( \frac{\partial^2}{\partial \tau^2} + \frac{1}{r^2} \right) (E_z + B_z) \quad (37)$$

which is the sum of Equations 32 and 33 evaluated for the azimuthal field dependences given following Equation 29.

$$E_\theta^{(e)} - B_\theta^{(e)} = 2a^2 \frac{\partial^2}{\partial \tau^2} \gamma \ln b/r + \gamma \frac{a^2}{r^2} \quad (38)$$

Note that the drift tube radius  $b$  appears logarithmically in the first term of Equation 38. That term is not necessarily small and cannot be dropped. The vacuum fields are derived for arbitrary  $b/a$  in Chapter 6.

Three matching conditions at the channel boundary are necessary to determine the  $\tau$ -dependent quantities  $\alpha$ ,  $\beta$  and  $\gamma$ .

$$E_z^{(e)} = E_z^{(i)} \quad (39)$$

$$B_z^{(e)} = B_z^{(i)} \quad (40)$$

$$\frac{\partial}{\partial \tau} (E_\theta^{(e)} - B_\theta^{(e)}) = - \frac{1}{\sigma} \frac{\partial}{\partial \tau} \frac{1}{r} \frac{\partial}{\partial r} r (E_z^{(i)} + B_z^{(i)}) - \frac{\partial}{\partial r} E_z^{(i)} \quad (41)$$

Equation 41 follows from continuity of  $E_\theta - B_\theta$ , and from Equations 21 and 23.

The jump conditions Equations 39-41 can, of course, also be treated as boundary conditions on the interior solutions by eliminating the exterior solutions.

$$E^{(i)} = B^{(i)} \quad (42)$$

$$2a^2 \ln b/a \frac{\partial^2}{\partial \tau^2} E_z^{(i)} + \frac{a}{\sigma} \frac{\partial}{\partial \tau} \frac{1}{r} \frac{\partial}{\partial r} r \left( E_z^{(i)} + B_z^{(i)} \right) + a \frac{1}{r} \frac{\partial}{\partial r} r E_z^{(i)} = 0 \quad (43)$$

The tracking force is now obtained. Substituting  $E_z$  and  $B_z$  from Equations 28, 29, and 36 into Equations 39 and 40 gives  $\beta = \gamma$  and

$$\frac{\partial}{\partial \tau} \beta = \frac{\partial}{\partial \tau} \alpha - \frac{\sigma}{a} S \quad (44)$$

Equations 28, 29, 38, 41 and 44 then yield a differential equation for  $\alpha$ ,

$$\left( \frac{\chi}{\sigma} \frac{\partial^2}{\partial \tau^2} + 2 \frac{\partial}{\partial \tau} + \sigma \right) \alpha = \left( \frac{\chi}{a} \frac{\partial}{\partial \tau} + \frac{\sigma}{a} \right) S \quad (45)$$

where

$$\chi \equiv \sigma^2 a^2 \ln b/a \quad (46)$$

The solution to Equation 45 is

$$\alpha = \frac{2\epsilon}{a^2} \int_0^\tau \left\{ e^{-\sigma(\tau-\tau')/\chi} \left[ \cosh \frac{\sqrt{1-\chi}}{\chi} \sigma(\tau-\tau') \right. \right. \\ \left. \left. + \frac{1}{\sqrt{1-\chi}} \sinh \frac{\sqrt{1-\chi}}{\chi} \sigma(\tau-\tau') \right] - e^{-\sigma(\tau-\tau')} \right\} \frac{\partial}{\partial \tau'} I d\tau' \quad (47)$$

The net angle-averaged dipole field acting on the beam is  $1/2(E_r - B_\theta - E_\theta - B_r)$ . This quantity is expressed in terms of  $E_z$  by using Equations 14 and 16.

$$\frac{\partial}{\partial \tau} (E_r - B_\theta - E_\theta - B_r) = -\frac{1}{r} \frac{\partial}{\partial r} r E_z \quad (48)$$

As in Chapter 2, the term proportional to  $\underline{S}$  in  $E_z$  does not contribute to tracking. Hence, the Frozen Field Tracking Model force is  $-aI$ .

For subsequent comparison with IPROP data, the separate electric and magnetic tracking force components are useful. The transverse fields inside the channel are obtained from Equations 20-23.

$$E_r = -E_\theta = -\alpha - \frac{\chi}{\sigma^2} \frac{\partial^2}{\partial \tau^2} \beta \quad (49)$$

$$B_r = B_\theta = -\frac{\chi}{\sigma^2} \frac{\partial^2}{\partial \tau^2} \beta \quad (50)$$

Inserting  $\alpha$  and  $\beta$  from Equations 44 and 45 then gives

$$\begin{aligned} \frac{1}{2} (E_r - E_\theta) &= \frac{2\epsilon}{a^2} \int_0^\tau \left\{ e^{-\sigma(\tau-\tau')/\chi} \frac{2}{\sqrt{1-\chi}} \sinh \frac{\sqrt{1-\chi}}{\chi} \sigma(\tau - \tau') \right. \\ &\quad \left. - e^{-\sigma(\tau-\tau')} \right\} \frac{\partial}{\partial \tau'} I \, d\tau' \quad (51) \end{aligned}$$

$$\begin{aligned} \frac{1}{2} (-B_r - B_\theta) &= \frac{2\epsilon}{a^2} \int_0^\tau e^{-\sigma(\tau-\tau')/\chi} \left[ \cosh \frac{\sqrt{1-\chi}}{\chi} \sigma(\tau - \tau') \right. \\ &\quad \left. - \frac{1}{\sqrt{1-\chi}} \sinh \frac{\sqrt{1-\chi}}{\chi} \sigma(\tau - \tau') \right] \frac{\partial}{\partial \tau'} I \, d\tau' \quad (52) \end{aligned}$$

Multiplied by  $-I$ , these are the electric and magnetic forces, respectively. It is evident from Equations 51 and 52 that the electric force is detracking, and the magnetic force tracking, at early times.

It is clear from Equations 10 and 45 that the Frozen Field Model tracking force must reduce to the Electrostatic Model tracking force as

$\chi \rightarrow 0$ . The magnetic component, Equation 52, vanishes, while the electric component, Equation 51, approaches the electrostatic force, Equation 11. This convergence is not uniform, however. Tracking at the very front of the beam is modified by magnetic effects for a distance in  $\tau$  of order  $\chi/\sigma$  no matter how small  $\chi$  becomes. Of course, strong modifications over very short distances have little practical importance.

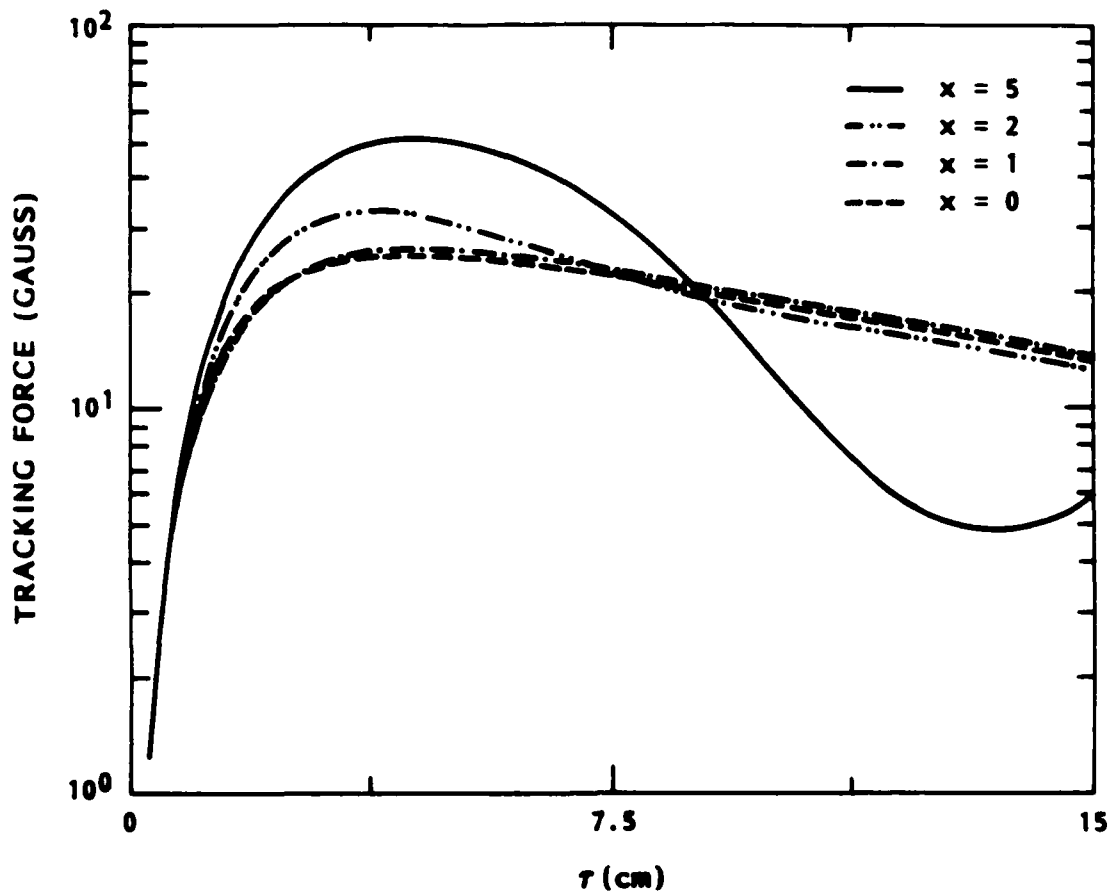
Although perhaps not immediately obvious, the tracking force expressions are continuous through  $\chi = 1$ . At  $\chi = 1$ , Equation 47 becomes

$$\alpha = \frac{2\epsilon}{a^2} \int_0^{\tau} e^{-\sigma(\tau-\tau')} \sigma(\tau - \tau') \frac{\partial}{\partial \tau'} I d\tau' \quad (53)$$

The analytic extension of Equation 47 above  $\chi = 1$  is obtained by replacing  $(1 - \chi)^{1/2}$  by  $(\chi - 1)^{1/2}$  and the hyperbolic functions by the corresponding trigonometric functions. Thus, the tracking force can oscillate in amplitude for  $\chi > 1$ . Eventually, dropping the diffusion terms from Equations 24 and 25 becomes inaccurate as  $\chi$  is increased.

The variation of the predicted tracking force with  $\chi$  for a 10 kA, 15 cm rise length beam offset 0.25 cm in a 1 cm radius,  $1 \text{ cm}^{-1}$  constant conductivity channel is illustrated in Figure 2. The force is nearly independent of  $\chi$  and equal to the Electrostatic Tracking Model force for  $\chi < 2$ . A stronger but oscillatory force arises at larger  $\chi$ . Note that the 25-50 g peak tracking forces should not be expected for more realistic beam and channel profiles.

The similarity between tracking force predictions from the Electrostatic and Frozen Field models suggested in Figure 2 does not carry over to their electric and magnetic components. Figure 3 depicts the tracking force components from Equations 51 and 52 for the beam and channel of Figure 2 but with  $\sigma = 0.5 \text{ cm}^{-1}$ ;  $\chi = 1$ . For a distance into the pulse of order a few times  $\chi/\sigma$ , the magnetic component clearly dominates. In fact, the electric component is detracking for a short distance. The early-time



R-899

FIGURE 2. THE FROZEN FIELD TRACKING MODEL NORMALIZED FORCE ( $-\alpha$  FROM EQ. 47) ON A 10 kA, 15 cm RISE LENGTH, 0.5 cm RADIUS BEAM OFFSET  $\epsilon = 0.25$  cm IN AN  $a = 1$  cm,  $\sigma = 1$  cm<sup>-1</sup> CONSTANT CONDUCTIVITY CHANNEL FOR  $x = 0, 1, 2,$  AND  $5$ . THE  $x = 0$  LIMIT CORRESPONDS TO THE ELECTROSTATIC TRACKING MODEL RESULT.

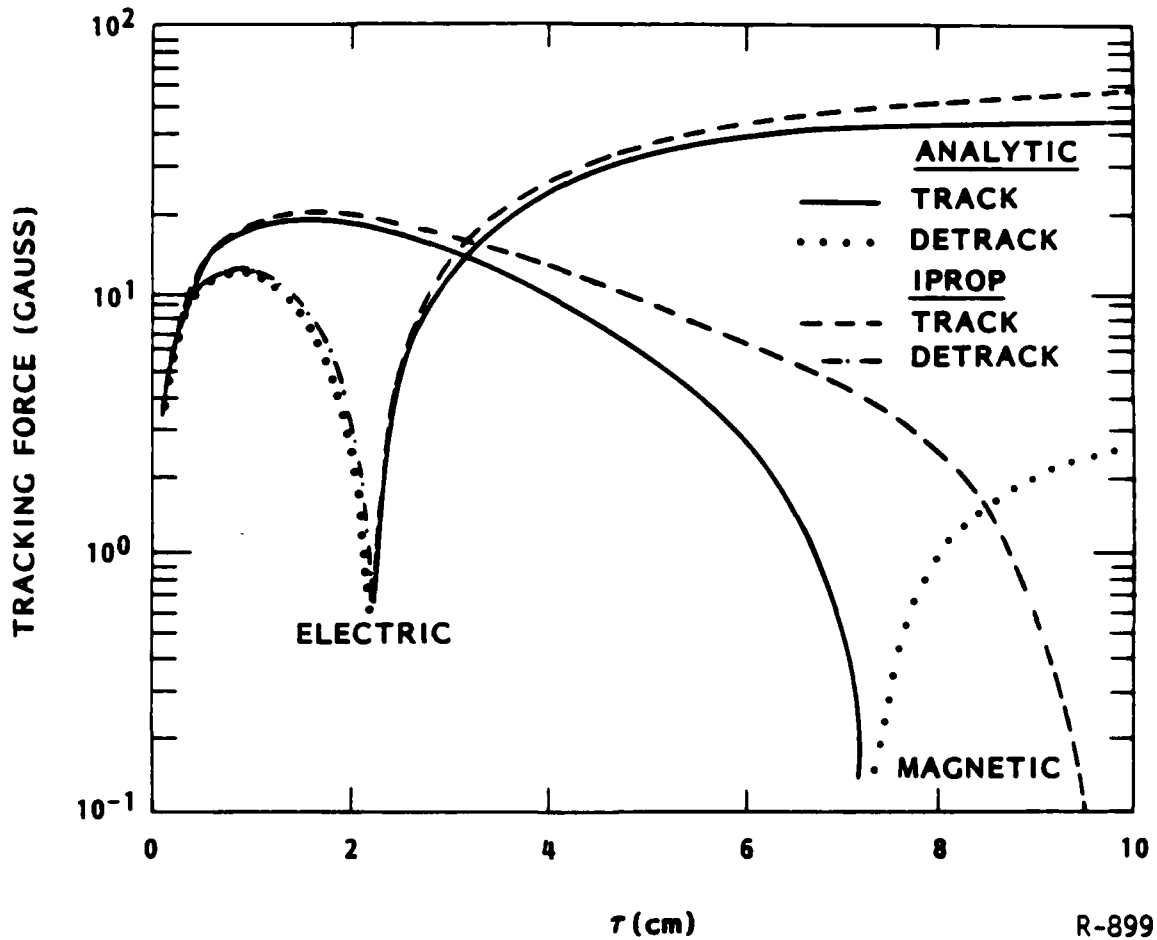


FIGURE 3. THE ELECTRIC AND MAGNETIC COMPONENTS OF THE NORMALIZED TRACKING FORCE ON A 10 kA, 15 cm RISE LENGTH, 0.5 cm RADIUS BEAM OFFSET  $\epsilon = 0.25$  cm IN AN  $a = 1$  cm,  $\sigma = 0.5$  cm $^{-1}$  CONSTANT CONDUCTIVITY CHANNEL FOR  $X = 1$ . THE FORCES ARE OBTAINED BOTH FROM EQUATIONS 51 AND 52 AND FROM A COMPARABLE IPROP SIMULATION.

magnetic tracking appears to be due both to lateral plasma currents and to the axial displacement current. Inductive effects cause the electric tracking reversal at the beam front. The remarkable cancellation between the components which allows the total tracking force to so nearly equal the purely electrostatic result from Chapter 2 may not persist for more realistic channel profiles.

Also plotted in Figure 3 are the tracking forces from a comparable IPROP simulation. Agreement is very good overall, supporting the validity of our tracking model. Radial profiles of the various fields in IPROP agree well with the predictions of Equations 20-23. IPROP preliminary tracking results are presented in some detail in Reference 1.

CHAPTER 4  
CHANNEL TRACKING WITH THE NEW FIELD EQUATIONS

Deriving the tracking force implied by the New Field Equations<sup>11</sup> is desirable, because this approximation to the Frozen Field Equations is used in many propagation codes. The New Field Equations can be written in many equivalent forms, including<sup>3</sup>

$$\frac{\partial}{\partial \tau} \nabla_{\perp}^2 (A_z - \phi) = \nabla_{\perp} \cdot \sigma \nabla_{\perp} \phi \quad (54)$$

$$\frac{\partial^2}{\partial \tau^2} (A_z - \phi) + \sigma \frac{\partial}{\partial \tau} (A_z - \phi) - \nabla_{\perp}^2 A_z = J \quad (55)$$

The axial displacement current, sometimes used in DYNASTY II,<sup>10</sup> is added to Equation 55. From time to time during the derivation which follows, we note the effects of dropping this term. In this way the tracking forces for the New Field Equations with and without the axial displacement current are obtain simultaneously.

Inside the channel, where  $\sigma$  is constant, Equations 54 and 55 can be manipulated to provide an equation for  $A_z - \phi$  alone.

$$\frac{\partial}{\partial \tau} \left( \frac{\partial}{\partial \tau} + \sigma \right) (A_z - \phi) = \left( 1 + \frac{1}{\sigma} \frac{\partial}{\partial \tau} \right) \nabla_{\perp}^2 (A_z - \phi) + J_z \quad (56)$$

Either  $A_z$  or  $\phi$  can be taken as the second dependent variable. We choose  $A_z$ .

$$\nabla_{\perp}^2 A_z = \left( 1 + \frac{1}{\sigma} \frac{\partial}{\partial \tau} \right) \nabla_{\perp}^2 (A_z - \phi) \quad (57)$$

As in the preceding derivations, Equation 56 is simplified by integrating once in  $\tau$ ,

$$\left(\sigma \frac{\partial}{\partial \tau} - \nabla_{\perp}^2\right) (A_z - \phi) = \sigma \int_0^{\tau} e^{-\sigma(\tau-\tau')} J d\tau' \quad (58)$$

Note that the first term in Equation 58 has a more complicated form in the absence of the axial displacement current. However, as before, we drop this diffusion term. In other words, the axial displacement current plays no direct role inside the channel.

$$\nabla_{\perp}^2 (A_z - \phi) = -\sigma \int_0^{\tau} e^{-\sigma(\tau-\tau')} J d\tau' \quad (59)$$

Equations 59 and 57 have dipole solutions

$$A_z^{(i)} - \phi^{(i)} = -\alpha r + \sigma \int_0^{\tau} S d\tau' \quad (60)$$

$$A_z^{(i)} = \left(1 + \frac{1}{\sigma} \frac{\partial}{\partial \tau}\right) (A_z^{(i)} - \phi^{(i)}) + \beta r \quad (61)$$

In the vacuum region outside the channel, Equations 54 and 55 reduce to

$$\nabla_{\perp}^2 (A_z - \phi) = 0 \quad (62)$$

$$\nabla_{\perp}^2 A_z = \frac{\partial^2}{\partial \tau^2} (A_z - \phi) \quad (63)$$

Their dipole solutions are

$$A_z^{(e)} - \phi^{(e)} = \gamma \frac{a^2}{r} \quad (64)$$

$$A_z^{(e)} = \delta \frac{a^2}{r} - \frac{\partial^2}{\partial \tau^2} \gamma \frac{ra^2}{2} \ln b/r \quad (65)$$

As in Chapters 2 and 3, small terms scaling as  $(a/b)^2$  are omitted. The second term in Equation 65 arises from the axial displacement current.

Four matching conditions at the channel boundary are needed to evaluate  $\alpha$ ,  $\beta$ ,  $\gamma$ , and  $\delta$ .  $A_z$  and  $\phi$  are continuous there. Integrating Equations 54 and 55 across the boundary gives, in addition,

$$\frac{\partial}{\partial r} A_z^{(e)} = \frac{\partial}{\partial r} A_z^{(i)} \quad (66)$$

$$\frac{\partial}{\partial \tau} \frac{\partial}{\partial r} (A_z^{(e)} - \phi^{(e)}) = \frac{\partial}{\partial \tau} \frac{\partial}{\partial r} (A_z^{(i)} - \phi^{(i)}) - \sigma \frac{\partial}{\partial r} \phi^{(i)} \quad (67)$$

Combining these with Equations 64 and 65 to eliminate the exterior fields yields

$$a(\ln b/a - 1/2) \frac{\partial^2}{\partial \tau^2} (A_z^{(i)} - \phi^{(i)}) + \frac{1}{r} \frac{\partial}{\partial r} r A_z^{(i)} = 0 \quad (68)$$

$$\left(\frac{\partial}{\partial \tau} + \sigma\right) \frac{\partial}{\partial r} (A_z^{(i)} - \phi^{(i)}) + \frac{1}{a} \frac{\partial}{\partial \tau} (A_z^{(i)} - \phi^{(i)}) - \sigma \frac{\partial}{\partial r} A_z^{(i)} = 0 \quad (69)$$

If desired,  $A_z^{(i)}$  also can be eliminated, leaving a single boundary condition at  $r = a$ .

$$a(\ln b/a - 1/2) \frac{\partial^2}{\partial \tau^2} (A_z^{(i)} - \phi^{(i)}) + \frac{1}{\sigma} \left(\frac{\partial}{\partial \tau} + \sigma\right) \frac{1}{r} \frac{\partial}{\partial r} r (A_z^{(i)} - \phi^{(i)}) + \frac{2}{\sigma a} \frac{\partial}{\partial \tau} (A_z^{(i)} - \phi^{(i)}) = 0 \quad (70)$$

The second-derivative terms in Equations 68 and 70 are omitted in the case of no axial displacement current.

Inserting Equations 60 and 61 into Equations 68 and 69, or Equation 60 into Equation 70 yields a differential equation for  $\alpha$  identical to Equation 45 for the Frozen Field Tracking Model but with  $X$  redefined as

$$\chi = \frac{1}{2} \sigma^2 a^2 (\ln b/a - 1/2) \quad (71)$$

With no axial displacement current,  $\chi = 0$ . The tracking fields are obtained by taking the gradient of  $-ar \cdot \cos\theta$ . When averaged in angle and summed, they give a tracking force  $-aI$ , as before. For completeness, we note that the electric and magnetic components of the tracking force are given by Equations 51 and 52 with  $\underline{\chi}$  from Equation 71.

In summary, the New Field Equations give rise to a tracking force equal to that of the Frozen Field Tracking Model (with  $\underline{\chi}$  reduced by approximately one-half) or that of the Electrostatic Tracking Model, depending on whether the axial displacement current is included. This progression  $\chi \rightarrow 1/2\chi \rightarrow 0\chi$  is associated with dropping first  $\partial B_z / \partial t$  and then  $\partial E_z / \partial t$  from the vacuum field equations and probably is due to the reduced field energy there. The plasma currents both drive and are, in part, driven by this field energy, which is proportional to  $\ln(b/a)$ .

CHAPTER 5  
DIFFUSION CORRECTIONS

Diffusion terms were ignored in previous sections in order to obtain analytically tractable results. Here, we evaluate the Laplace transforms of the tracking forces with the diffusion terms retained in order to estimate their importance. The transformed tracking forces can be derived by paralleling the derivations in Chapters 3 and 4, starting from the transforms of Equations 24 and 25 for the Frozen Field model and Equation 58 for the New Field models. Indeed, we have done so and obtained the results given below. Here, however, we outline an alternative, more formal approach.

Throughout this section, all quantities are taken to be Laplace-transformed with respect to  $\tau$ . The transform variable is  $\underline{s}$ .

In coordinates centered on the channel axis, the net tracking force consists of a monopole force acting on the beam dipole current and a dipole force acting on the beam monopole current. The dipole current is given by  $-\epsilon \partial J / \partial r$  for a rigidly displaced beam. Thus, the total force, averaged over angle and normalized to the beam current, is

$$I^{-1} \int \left[ F_0 \left( -\epsilon \frac{\partial J}{\partial r} \right) + F_1 J \right] r' dr' \quad (72)$$

The forces can, in turn, be expressed in terms of potentials,

$$F_0 = \frac{\partial}{\partial r} \zeta_0 \quad (73)$$

$$F_1 = \frac{1}{r} \frac{\partial}{\partial r} r \zeta_1 \quad (74)$$

Inserting Equations 73 and 74 into Equation 72 and integrating by parts gives

$$-I^{-1} \int \left( \zeta_1 + \epsilon \frac{\partial}{\partial r} \zeta_0 \right) \left( \frac{\partial}{\partial r} J_r \right) r' dr' \quad (75)$$

The integrand of Equation 75 would, of course, vanish identically were it not for the channel edge.

Now let us suppose that the potentials satisfy

$$\left( \frac{1}{r} \frac{\partial}{\partial r} r \frac{\partial}{\partial r} - \kappa^2 - \frac{m^2}{r^2} \right) \zeta_m = -J^{(m)} \frac{\sigma}{\sigma + s} \quad (76)$$

with boundary conditions

$$\zeta_0 + \eta_0 \frac{\partial}{\partial r} \zeta_0 = 0 \quad (77)$$

$$\zeta_1 + \eta_1 \frac{1}{r} \frac{\partial}{\partial r} r \zeta_1 = 0 \quad (78)$$

at the channel wall,  $r = a$ . These equations are solved conveniently in terms of Green's functions,

$$\zeta_m = - \frac{\sigma}{(\sigma + s)} \int G_m(r, r') J^{(m)}(r') r' dr' \quad (79)$$

$$G_m = \begin{cases} \frac{\pi}{2} J_m(\kappa r') \psi_m(\kappa r) & r > r' \\ \frac{\pi}{2} J_m(\kappa r) \psi_m(\kappa r') & r < r' \end{cases} \quad (80)$$

$$\psi_0 = Y_0(\kappa r) - J_0(\kappa r) \frac{Y_0(\kappa a) - \eta_0 \kappa Y_1(\kappa a)}{J_0(\kappa a) - \eta_0 \kappa J_1(\kappa a)} \quad (81)$$

$$\psi_1 = Y_1(\kappa r) - J_1(\kappa r) \frac{Y_1(\kappa a) + \eta_1 \kappa Y_0(\kappa a)}{J_1(\kappa a) + \eta_1 \kappa J_0(\kappa a)} \quad (82)$$

$J_m$  and  $Y_m$  are Bessel functions of the first and second kinds.<sup>12</sup>

The integrations in Equations 75 and 79 are straightforward, if the beam profile is square, so that  $\partial J / \partial r = -J \delta(r - a_b)$ .

$$\zeta_0 = -\frac{\pi}{2} \frac{\sigma}{\sigma + s} I \frac{J_1(\kappa a_b)}{1/2 \kappa a_b} \psi_0(\kappa r) \quad r \geq a_b \quad (83)$$

$$\zeta_1 = -\frac{\pi}{2} \frac{\sigma}{\sigma + s} I \kappa \epsilon \frac{J_1(\kappa a_b)}{1/2 \kappa a_b} \psi_1(\kappa r) \quad r \geq a_b \quad (84)$$

The tracking force is

$$-\frac{2\epsilon\sigma}{\sigma + s} \frac{I}{a^2} \left( \frac{J_1(\kappa a_b)}{1/2 \kappa a_b} \right)^2 \frac{(1 + \eta_0 \eta_1 \kappa^2) 1/2 \kappa a}{[J_1(\kappa a) + \eta_1 \kappa J_0(\kappa a)][J_0(\kappa a) - \eta_0 \kappa J_1(\kappa a)]} \quad (85)$$

The Bessel function Wronskian formula<sup>12</sup> was used in obtaining Equation 85.

It can be shown that  $\eta_0 = 0$  for the three tracking models investigated in this report. Physically, this corresponds to the vanishing of the axisymmetric portion of  $E_z$  outside the channel for ultrarelativistic beams. Equation 85 can be simplified notationally by absorbing the shape factor  $[J_1(\kappa a_b)/(1/2 \kappa a_b)]^2$  into  $I$ . This quantity is equal to unity at long transverse wavelengths, and decreases rapidly for  $1/2 \kappa a_b > 2.4$ . With these changes, Equation 85 becomes

$$-\frac{2\epsilon\sigma}{\sigma + s} \frac{I}{a^2} \frac{1/2 \kappa a}{J_0(J_1 + \eta_1 \kappa J_0)} \quad (86)$$

From here on, the Bessel function arguments are understood to be  $\kappa a$ .

For the Frozen Field Equations of Chapter 3,  $-E_z/s$  can be identified as the potential  $\zeta$ , and  $-\sigma s$  as  $\kappa^2$ . See Equations 24 and 48. Since  $B_z$  is proportional to  $J_m(\kappa a)$  inside the channel, Equations 42 and 43 can be combined to yield the boundary condition

$$(2Xs^2 + \sigma s J_0/J_1) E_z + \sigma a(\sigma + s) \frac{1}{r} \frac{\partial}{\partial r} r E_z = 0 \quad (87)$$

from which  $\eta_1$  can be identified. Consequently, the Laplace-transformed tracking force is

$$-\frac{2\epsilon}{a^2} \frac{s}{\sigma + s} I \frac{\left( Xs/J_0 + \sigma \frac{1}{2} \kappa a/J_1 \right) \sigma}{Xs^2 J_1 / 1/2\kappa a + \sigma(\sigma + 2s)J_0} \quad (88)$$

Similarly,  $A_z - \phi$  is the potential for the New Field Equations of Chapter 4. The transverse wavenumber  $\kappa^2$  is  $-\sigma$  if the axial displacement current is retained, and  $-\sigma/(\sigma + s)$  otherwise. See Equation 58 and the associated text. The Laplace-transform of Equation 70 provides the boundary condition. The resulting tracking force is

$$-\frac{2\epsilon}{a^2} \frac{s}{\sigma + s} I \frac{(Xs + \sigma)\sigma}{J_0[(Xs^2 + \sigma s)J_1 / 1/2\kappa a + \sigma(\sigma + s)J_0]} \quad (89)$$

Recall that  $\underline{X}$  is set to zero, if the axial displacement current is dropped.

Setting  $J_0$  and  $J_1 / 1/2\kappa a$  to unity in either Equation 88 or 89 yields

$$-\frac{2\epsilon}{a^2} \frac{s}{\sigma + s} I \frac{(Xs + \sigma)\sigma}{Xs^2 + 2\sigma s + \sigma^2} \quad (90)$$

This is the Laplace transform of Equation 47, the channel tracking force derived with the diffusion term ignored inside the channel, as can be seen most readily by examining Equations 8 and 45. Thus, dropping the diffusion term is valid if  $|s_1| < 4/\sigma a^2$ , or  $4\sigma/(\sigma^2 a^2 + 1)$  for the New Field Equations without the axial displacement current.  $s_1$  is a zero of  $Xs^2 + 2\sigma s + \sigma^2$ . Numerical analysis of the poles and residues of Equations 88 and 89 indicates that the factor 4 can be increased to  $2.4^2$ .

In Chapters 3 and 4 and again here, it is seen that the tracking forces for the Frozen Field Equations and for the New Field Equations with the axial displacement current are formally identical when the diffusion term is omitted, differing only in the definitions of  $X$ . The complete force expressions, Equations 88 and 89, are not formally identical, however. Nonetheless, their lowest poles and corresponding residues are

nearly equal numerically, at least for  $\sigma^2 a^2 < 10$ . The tracking force for the New Field Equations without the axial displacement current is, of course, qualitatively different from that of the other models, unless  $X \ll 1$ : the lowest poles are a complex conjugate pair in the first two cases and a single real value in the third.

Further numerical investigation of the poles and residues yields a result which is surprising at first sight. The lowest poles, in terms of  $\text{Re}(s_j)$ , contribute to tracking, or in the case of complex conjugate pairs contribute alternately (in  $\tau$ ) to tracking and detracking, but tracking first. The lowest pole associated with detracking comes from the smallest zero of the factor  $J_0$  in the denominators of Equations 88 and 89 and so has a large  $\text{Re}(s_j)$ . (It represents beam repulsion from the channel due to the monopole return current.) This seems to predict that beams always track conductivity channels, independent of the magnitude of  $\sigma a$ . This apparent discrepancy with simulation results probably is resolved as follows. The complex conjugate pair which occurs for  $X \neq 0$  has a very large imaginary part for  $\sigma a$  very large. Thus, the tracking force oscillates rapidly in sign, so that its average value is small. In addition, the corresponding residues become very small. When  $X = 0$ , on the other hand, the lowest tracking pole moves very close to the first detracking pole as  $\sigma a$  becomes large, and their effects approximately cancel. The behavior of higher poles then must be considered. We have not done so, because it does not seem worthwhile.

Incidentally, the next higher tracking pole in Equations 88 and 89 takes on the value  $3.8^2/\sigma a^2$  for  $\sigma a$  small and gradually decreases to  $2.4^2/\sigma a^2$  as  $\sigma a$  becomes very large. It is probably this pole that enters into the resistive hose instability.

CHAPTER 6  
CONDUCTING-WALL CORRECTIONS

The conducting drift tube surrounding the beam channel enters the preceding calculations only through the logarithm appearing in  $\chi$ . Other terms, of order  $(a/b)^2$  or smaller, are ignored. Now, we repeat the analysis of Chapter 3 with these terms included to demonstrate that they are, indeed, unimportant for large drift tubes. The impact of a small drift tube on channel tracking also is determined.

General solutions to Equations 30 and 31 for  $E_z$  and  $B_z$  in vacuum between  $\underline{a}$  and  $\underline{b}$  with  $E_z(b) = 0$  are

$$E_z^{(e)} = \frac{\partial}{\partial \tau} \gamma a \left( \frac{a}{r} - \frac{a^2}{b^2} \frac{r}{a} \right) \quad (91)$$

$$B_z^{(e)} = \frac{\partial}{\partial \tau} \gamma a \left( \frac{a}{r} + \frac{a^2}{b^2} \frac{r}{a} \right) \quad (92)$$

The transverse fields are derived most easily by taking the sums and differences of Equations 32 and 33 and of Equations 34 and 35, and then integrating once each in  $\tau$  and  $\underline{r}$ .  $E_\theta(b) = 0$  determines one integration constant.

$$E_\theta^{(e)} = \frac{\partial^2}{\partial \tau^2} \gamma a^2 \left[ \ln b/r - 1/4 \left( \frac{r^2}{b^2} - 1 \right) \right] + \frac{1}{2} (\gamma + \sigma) \left( \frac{a^2}{r^2} - \frac{a^2}{b^2} \right) \quad (93)$$

$$B_\theta^{(e)} = \frac{\partial^2}{\partial \tau^2} \gamma a^2 \left[ -\ln b/r - 1/4 \left( \frac{r^2}{b^2} + 1 \right) \right] + \frac{1}{2} (-\gamma + \sigma) \left( \frac{a^2}{r^2} + \frac{a^2}{b^2} \right) \quad (94)$$

$$E_r^{(e)} = \frac{\partial^2}{\partial \tau^2} \gamma a^2 \left[ -\ln b/r - 1/4 \left( \frac{r^2}{b^2} + 1 \right) \right] + \frac{1}{2} (\gamma + \sigma) \left( \frac{a^2}{r^2} + \frac{a^2}{b^2} \right) \quad (95)$$

$$B_r^{(e)} = \frac{\partial^2}{\partial \tau^2} \gamma a^2 \left[ -\ln b/r + 1/4 \left( \frac{r^2}{b^2} - 1 \right) \right] + \frac{1}{2} (\gamma - \sigma) \left( \frac{a^2}{r^2} - \frac{a^2}{b^2} \right) \quad (96)$$

Matching these exterior solutions to the interior solutions, already given in Equations 28 and 29, is accomplished through continuity of  $E_z$  (Eq. 39),  $B_z$  (Eq. 40),  $E_\theta - B_\theta$  (Eq. 41), and  $E_\theta + B_\theta$

$$\frac{\partial}{\partial \tau} \left( E_\theta^{(e)} + B_\theta^{(e)} \right) = \frac{1}{\sigma} \frac{\partial}{\partial \tau} r \frac{\partial}{\partial r} \frac{1}{r} \left( E_z^{(i)} - B_z^{(i)} \right) + \frac{\partial}{\partial r} E_z^{(i)} \quad (97)$$

The counterpart of Equation 97 was not required in Chapter 3 due to a fortuitous cancellation. Combining all these equations yields after some algebra

$$\begin{aligned} & \left[ \frac{\chi}{\sigma} \frac{\partial}{\partial \tau^2} + 2 \frac{\partial}{\partial \tau} + \sigma \left( 1 - \frac{a^2}{b^2} \right) \right] \alpha \\ & = \left[ \frac{\chi}{a} \frac{\partial}{\partial \tau} + \frac{\sigma}{a} \left( 1 + \frac{a^2}{b^2} \right) \right] S + \frac{2\epsilon}{b^2} \sigma \left( 1 - \frac{a^2}{b^2} \right) I \end{aligned} \quad (98)$$

$\chi$  is again redefined.

$$\chi \equiv \sigma^2 a^2 \left[ \ln b/a + 1/4(1 - a^4/b^4) \right] \quad (99)$$

The primary difference between this formula and Equation 45, which was obtained in the limit of large  $b/a$ , is seen to be the additional source term, proportional to the beam current, on the right side of Equation 98. Other terms involving  $b$  can, in fact, be eliminated formally by renormalizing  $\alpha$ ,  $\chi$ ,  $\sigma$ , and  $\tau$ . The corrections involved are, in any event, small so long as  $(b/a)^2 \gg 1$ . Solving Equation 98 yields the additional contribution to the tracking force,

$$\frac{2\epsilon}{b^2} \int_0^\tau e^{-\sigma(\tau-\tau')/\chi} \frac{1}{\sqrt{1-\chi}} \sinh \frac{\sqrt{1-\chi}}{\chi} \sigma(\tau-\tau') \sigma I d\tau' \quad (100)$$

where terms of order  $(a/b)^2$  have been omitted. For  $\chi \ll 1$  this becomes

$$\frac{2\epsilon}{b^2} \int_0^{\tau} e^{-\sigma(\tau-\tau')/2} \frac{1}{2} \sigma I d\tau' \quad (101)$$

Both expressions reduce to  $2\epsilon I/b^2$ , the usual magnetic image force, for  $\sigma\tau_r \gg 2$ .  $\tau_r$  is the current rise length. The corresponding electric image is shielded by the channel conductivity at late times. Recall that these results assume  $\sigma a$  small in the sense of Chapter 5. The magnetic image force is reduced by return currents for  $\sigma a$  large.

The criterion  $\sigma\tau_r \gg 2$  for the magnetic wall force to reduce to  $2\epsilon I/b^2$  is almost always satisfied in practice. On this basis, it can be shown that the wall force on the beam head is small compared to the tracking force when  $(b/a)^2 \gg 10$ . That the wall force on the beam body be small compared to the tracking force requires that  $(b/a)^2$  be much greater than several times  $\sigma\tau_r$ , with the conductivity evaluated in the beam head. IPROP simulations suggest  $(b/a)^2 \gg 500$  for realistic beam and channel radial profiles with  $a = 1$  cm,  $\sigma = 1$  cm<sup>-1</sup>, and  $\tau_r = 100$  cm. It is desirable that the second, more restrictive, condition be met so that wall-force centering of the beam body not be confused with tracking of the beam head.

## CHAPTER 7 CONCLUSIONS

The foregoing calculations provide an improved model of conductivity channel tracking. The derivation is based on the complete set of Frozen Field Equations. It is valid for  $\sigma a < 2.4$  and  $b/a > 10$ , although  $b/a \gg 20$  probably is necessary for unambiguous experimental confirmation. The model also requires the beam to lie entirely within a sharp-edged constant conductivity channel. Note surprisingly, simulations show somewhat weaker tracking forces for more realistic conditions. Qualitative features of the model nonetheless persist.

The analytical tracking force expression contains a quantity  $\underline{X}$  which measures the electromagnetic tracking-field energy outside the channel. For  $X < 1$  the tracking force is approximately that of the Electrostatic Tracking Model. For  $X > 1$ , on the other hand, the tracking force oscillates in time like an underdamped pendulum. This field energy can be thought of as inertia of the tracking force. Dropping  $B_z$ , which is done in the New Field Equations with the displacement current retained, cuts this inertia in half. Dropping the displacement current as well eliminates the inertia entirely.

$\underline{X}$  diverges logarithmically for large drift tube radii. This seemingly nonphysical result is a consequence of the ultrarelativistic approximation implicit in the Frozen Field Equations. A Lorentz transformation to the beam frame shows in a qualitative sense that  $\underline{b}$  should be replaced by  $\gamma\tau_0$  in open air.  $\tau_0$  is the axial scale length over which the tracking force varies; it is smaller than  $\tau_r$ . Fields tend to fall off spherically rather than cylindrically at radii greater than  $\gamma\tau_0$ . Values of  $\ln(\gamma\tau_0/a)$  larger than about 15 are unlikely in practice.

A distinctive feature of the Frozen Field Tracking Model is the role of transverse magnetic fields. Radial and azimuthal dipole plasma currents

near the beam head drive  $B_r$  and  $B_\theta$  via Faraday's law provided  $B_z$  is not set to zero. In addition, the dipole axial displacement current generates transverse magnetic fields irrespective of whether  $B_z = 0$ . It is not difficult to see that  $V \times B$  always leads to a centering force on the beam at early times, when the lateral plasma currents are still rising. Moreover, the force can be quite large. That the transverse electric fields should be modified inductively so that they largely cancel the magnetic force for  $X < 1$ , leaving a net tracking force not much different from that of the Electrostatic Tracking Model, is surprising. Whether this cancellation persists for more realistic channel profiles is unknown.

At least for the idealized conditions considered here, the New Field Equations describe channel tracking about as well as the complete Frozen Field Equations, provided the axial displacement current is retained in the New Field Equations. Omitting the displacement current changes tracking forces qualitatively. Physically, oscillations occurring for  $X > 1$  and early time magnetic field effects are lost. Mathematically, the complex conjugate pair of roots are replaced by a single real root in the plasma dielectric function. (This loss of a mode can be seen more simply by deriving the dispersion relation for normal modes of the New Field Equations, with and without the axial displacement current, in a homogeneous resistive medium.) At a minimum, the axial displacement current should be kept in any New Field Equation calculation of tracking. It seems prudent, more generally, to retain the axial displacement current whenever the condition  $\sigma a > 2$  is not well satisfied.

## REFERENCES

1. Welch, D. R. and Godfrey, B. B., Enhanced Channel Tracking Due to Beam-Generated Magnetic Fields, AMRC-R-814, Mission Research Corporation, Albuquerque, 1986.
2. Masamitsu, J. A., Yu, S. S., and Chambers, F. W., Beam Tracking Studies with RINGBEARER II, UCID-19771, Lawrence Livermore National Laboratory, Livermore, 1982.
3. Hui, B. and Lampe, M., Numerical and Analytical Studies of Beam Channel Tracking, NRL Report 5136, Naval Research Laboratory, Washington, 1984.
4. Lee, E. P., Calculation of a Tracking Force, UCID-19674, Lawrence Livermore National Laboratory, Livermore, 1983.
5. Hui, B., et al., in Proc. 1986 SDIO/DARPA/Services Beam Propagation Review, to be published.
6. Welch, D. R., private communication (1986).
7. Parkinson, E. R. and Keeley, D. A., Studies in High Current Beam Propagation at Reduced Pressures, SAIC-C-U-75-PA, Science Applications International Corporation, Palo Alto, 1985.
8. Godfrey, B. B., The IPROP Three-Dimensional Beam Propagation Code, AMRC-R-690, Mission Research Corporation, Albuquerque, 1985.
9. Chambers, F. W., Masamitsu, J. A., and Lee, E. P., Mathematical Models and Illustrative Results for the RINGBEARER II Monopole/Dipole Beam Propagation Code, UCID-19494, Lawrence Livermore National Laboratory, Livermore, 1984.
10. Hui, B. and Lampe, M., DYNASTY II, A Nonlinear Implicit Code for Relativistic Electron Beam Tracking Studies, NRL Report 5138, Naval Research Laboratory, Washington, 1983.
11. Lee, E. P., The New Field Equations, UCID-17286, Lawrence Livermore National Laboratory, Livermore, 1976.
12. Abramowitz, M. and Stegun, I. A. (eds.), Handbook of Mathematical Functions (U. S. Government Printing Office, Washington, 1964), Sec. 9.1.

END

7-87

DTIC